ELSEVIER

14 August 2000

Physics Letters A 273 (2000) 15–24

PHYSICS LETTERS A

www.elsevier.nl/locate/pla

New signal extraction scheme with harmonic demodulation for power-recycled Fabry–Perot–Michelson interferometers

Koji Arai [a,*], Masaki Ando [a], Shigenori Moriwaki [b], Keita Kawabe [a,1], Kimio Tsubono [a]

[a] *Department of Physics, University of Tokyo, 7-3-1 Hongo, Bunkyo-ku, Tokyo 113-0033, Japan*
[b] *Department of Advanced Materials Science, University of Tokyo, 7-3-1 Hongo, Bunkyo-ku, Tokyo 113-0033, Japan*

Received 25 May 2000; accepted 3 July 2000
Communicated by P.R. Holland

Abstract

We present a new signal-extraction scheme based on harmonic demodulation for control of a power-recycled interferometric gravitational-wave detector. Demodulation at the third-harmonic frequency of a frontal phase modulation is used to robustly extract well-separated longitudinal signals.

PACS: 04.80.Nn; 07.60.Ly; 95.55.Ym
Keywords: Gravitational wave detector; Interferometer; Fabry–Perot; Power recycling

1. Introduction

Several large- and middle-scale interferometric gravitational-wave detectors are currently being constructed by the LIGO [1], VIRGO [2], GEO [3], and TAMA [4] groups. These detectors utilize variants of a Michelson interferometer with suspended mirrors to detect the differential arm-length changes induced by gravitational waves from astrophysical sources. The LIGO, VIRGO and TAMA detectors are Fabry–Perot–Michelson interferometers; these detectors have Fabry–Perot cavities in their arms to enhance the phase change caused by gravitational waves. In addition, in order to increase the laser power inside the interferometer, all detectors use the technique of power recycling [5].

Power recycling is implemented by inserting an additional partially transmitting mirror in front of the interferometer (recycling mirror RM in Fig. 1); it forms the so-called recycling cavity together with the rest of the interferometer, which serves as a compound mirror. When the output port is kept on a dark fringe, most of the light returning from the arms is directed back to the laser source. The recycling mirror reflects this light back towards the beamsplitter, adding it to the input laser beam. The resulting increase in effective input power improves the shot-

* Corresponding author. Current address: Space-time Astronomy Section, National Astronomical Observatory, 2-21-1 Osawa, Mitaka-shi, Tokyo 181-8588, Japan.
E-mail address: koji.arai@nao.ac.jp (K. Arai).
[1] Current address: Max-Planck-Institut für Quantenoptik, D-85748 Garching bei München, Germany.

0375-9601/00/$ - see front matter
PII: S0375-9601(00)00467-9

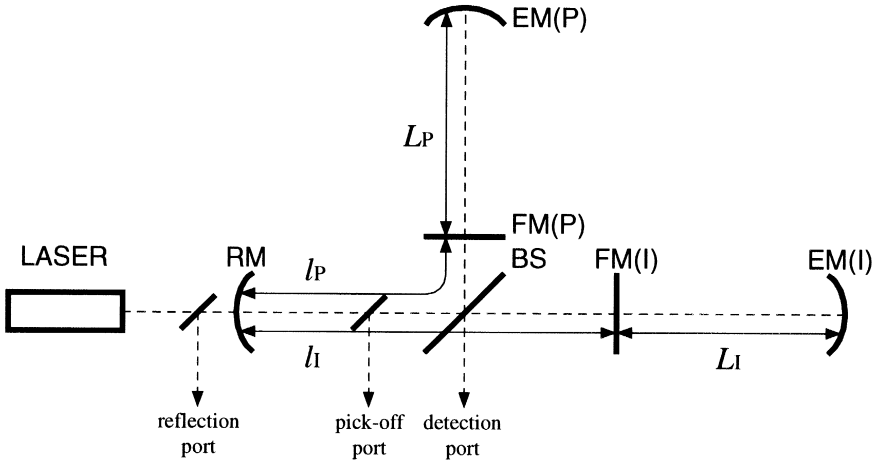

Fig. 1. Optical layout of a power-recycled Fabry–Perot–Michelson interferometer. RM, recycling mirror; BS, beamsplitter; FM, front mirror (I - Inline, P - Perpendicular); and EM, end mirror.

noise-limited sensitivity of the instrument. At present, power recycling is an indispensable technique for the interferometric gravitational wave detectors because the output power of their laser sources is insufficient to achieve the desired sensitivity.

A power-recycled Fabry–Perot–Michelson interferometer has four longitudinal degrees of freedom: the fluctuations of the arm cavity lengths (δL_I and δL_P in Fig. 1) and those of the distances between the recycling mirror and the front mirrors (δl_I and δl_P in Fig. 1). These degrees of freedom can also be represented by the linear combinations:

$$\begin{aligned}
\delta L_- &= \delta L_P - \delta L_I\,, \\
\delta L_+ &= \delta L_P + \delta L_I\,, \\
\delta l_- &= \delta l_P - \delta l_I\,, \\
\delta l_+ &= \delta l_P + \delta l_I\,. \qquad (1)
\end{aligned}$$

During the operation of the interferometer, the input laser beam needs to be kept resonant in both arm cavities and the recycling cavity, and the interference fringe has to be kept dark at the detection port. Since seismic excitation induces motions of the suspended mirrors larger than the wavelength of the laser, the operating point for those four degrees of freedom is maintained by feedback controls.

Fig. 2 (excluding the components inside of the dashed box) shows the conventional frontal modulation scheme for a power-recycled Fabry–Perot–Michelson interferometer [6–8]. This scheme employs a combination of a variant of the reflection sensing technique [9] and a frontal (or Schnupp) modulation [10,11]; phase modulation at a radio frequency (ω_m) is applied to the beam incident on the recycling mirror, and a macroscopic asymmetry (l_-) between l_P and l_I – the so-called Schnupp asymmetry – is intentionally introduced. The longitudinal signals necessary for maintaining all of the four degrees of freedom are obtained by demodulating the outputs of several photodetectors, where intensity-modulated photocurrents are induced by fluctuations of the mirrors from the operating point. With the conventional frontal modulation scheme, however, a δl_+ signal is not obtained independently from the δL_+ signal; those signal extraction ports sensitive to δl_+ are also highly sensitive to δL_+. In addition, the δl_+ and δl_- signals may vanish under some conditions that are described later.

In order to overcome these problems, a technique that does not require any modification of the basic optical configuration for the frontal modulation was presented in [6]. This technique uses feedback control to the δL_+ and δl_+ loops with different gains, accepting several restrictions to ensure the stability of the control system. Also, the optical parameters must be chosen carefully to avoid the conditions that make the longitudinal signals disappear. As more fundamental solutions to the problems, several tech-

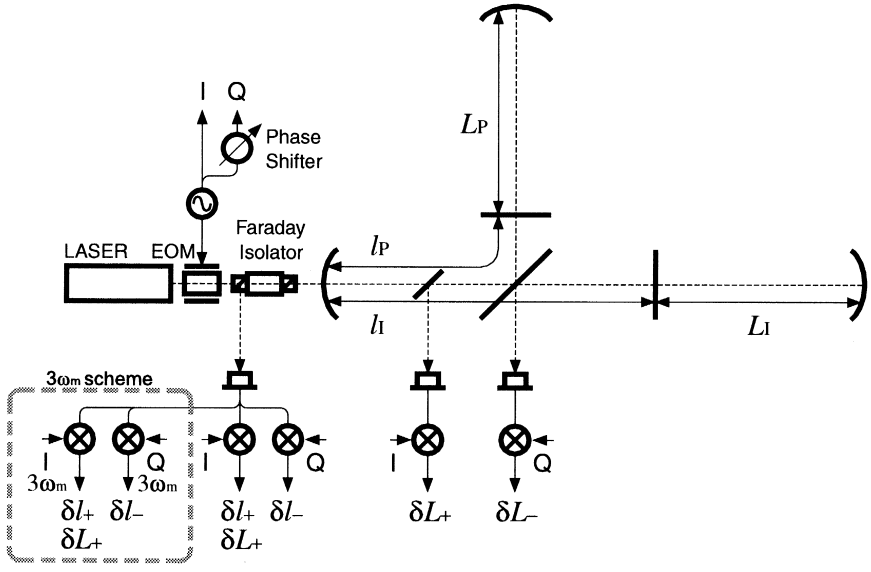

Fig. 2. Signal extraction scheme of power-recycled Fabry–Perot–Michelson interferometer. The components in the dashed box are the signal-extraction ports for the $3\omega_m$ demodulation proposed in this article. The symbols I and Q represent the local oscillators whose initial phase is same (in-phase) and orthogonal (quadrature-phase) as the phase modulation.

niques to separate the longitudinal signals have been investigated. Signal extraction schemes using a frequency-shifted subcarrier, which is generated by an additional modulation and a complex input optics assembly, have been described in several papers [8,12,13]. In our earlier Letters [14,15], we have presented and demonstrated a technique to obtain a δl_+ signal without the contribution of δL_+ by precisely adjusting the optical parameters.

Here, we propose a new signal extraction scheme for power-recycled Michelson interferometers with Fabry–Perot arms based on frontal modulation. The signals corresponding to δl_+ and δl_- are obtained at the reflection port by demodulation at the third-harmonic of the modulation frequency – hereafter we call this demodulation '$3\omega_m$ demodulation'. This technique can be realized without either an additional modulation or a modification of the basic optical configuration as used in the conventional scheme. The extracted δl_+ signal inherently has better separation from δL_+ than the signal with the ω_m demodulation. In addition, several options are available to completely eliminate the δL_+ contribution from the demodulated signals. The amplitudes and the signs of the δl_+ and δl_- signals with the $3\omega_m$ scheme have a smaller dependence on the optical parameters as compared to the conventional ω_m demodulation; the signals do not vanish for typical optical parameters. Consequently, the control system with our technique is greatly simplified and becomes robust against fluctuations of the optical parameters caused by contamination of the mirror surfaces and by imperfections of the interferometer such as misalignments.

2. Signal extraction with frontal modulation scheme

2.1. Frontal modulation

The phase modulation at a radio frequency ω_m generates sidebands separated from the carrier frequency Ω by $n\omega_m$ ($n = \pm 1, \pm 2, \ldots$). The resulting electric field of the beam is expressed as the superposition of the carrier and the nth order sidebands given by $E_l\, i^n J_n(m) e^{i(\Omega + n\omega_m)t}$, where E_l is the amplitude of the incident electric field, m is the modulation index, and $J_n(m)$ is the nth-order Bessel function. At the operating point, the carrier is kept

Table 1
Resonant conditions of the carrier and the sidebands in the recycling cavity (RC) and the arm cavities.

Order	resonance in the arms by the arms	phase shift	phase shift in RC	resonance in RC
0	resonant	0	0	resonant
1	non-resonant	π	π	resonant
2	non-resonant	π	2π	non-resonant
3	non-resonant	π	3π	resonant

resonant with both the recycling cavity and the arm cavities. In addition, an interference fringe for the carrier at the detection port is kept dark. On the other hand, the first-order sidebands are resonant only with the recycling cavity. Because of the intentional Schnupp asymmetry, a fraction of the first-order sidebands leaks out even for the dark fringe of the carrier, leading to a signal which is sensitive to a deviation from the dark fringe for the carrier induced by gravitational waves.

The amplitude reflectivity of the arm is a function of the round-trip-phase ϕ in the arm, that is,

$$r_{\mathrm{arm}}(\phi) = -r_{\mathrm{F}} + \frac{t_{\mathrm{F}}^2 r_{\mathrm{E}} \mathrm{e}^{-\mathrm{i}\phi}}{1 - r_{\mathrm{F}} r_{\mathrm{E}} \mathrm{e}^{-\mathrm{i}\phi}}\,, \tag{2}$$

where r and t represent the amplitude reflectivity and transmissivity, and the subscripts F and E indicate the front mirror and the end mirror, respectively. The carrier is kept resonant in the arm ($\phi = 0 \bmod 2\pi$), and all of the sidebands are kept approximately anti-resonant with the arm ($\phi \sim \pi \bmod 2\pi$). The two arms are designed to be definitely over-coupled for the resonant carrier because the reflectivity of each end mirror is made as high as possible in order to minimize losses caused by transmission through the end mirrors. In this configuration the reflectivity of the arm for the sidebands ($r_{\mathrm{arm}\,n}$) – $n \neq 0$ – is unity, while that for the carrier ($r_{\mathrm{arm}\,0}$) is also roughly unity – however smaller than that of the sidebands and with the opposite phase. The response of the arm to fluctuations of the arm length is represented by the derivative of the arm reflectivity with respect to ϕ, that is,

$$r'_{\mathrm{arm}}(\phi) \equiv \frac{\partial r_{\mathrm{arm}}(\phi)}{\partial \phi}\,. \tag{3}$$

For the resonant carrier, this derivative becomes much larger than unity owing to the phase amplification by the cavities, while the derivatives for non-resonant sidebands becomes negligible compared with unity. Therefore we ignore $r'_{\mathrm{arm}\,n}$ for $n \neq 0$.

The resonant conditions for the carrier and the sidebands in the arms and the recycling cavity are summarized in Table 1. The modulation frequency and the average round-trip-length of the recycling cavity ($l_+ \equiv l_{\mathrm{I}} + l_{\mathrm{P}}$) are chosen such that the first-order sidebands resonate only with the recycling cavity. As we mentioned above, the sidebands acquire a phase shift of π relative to the carrier upon reflection from the arms. In order to achieve resonance of the first-order sidebands with the recycling cavity, l_+ is set such that the first-order sidebands experience an additional phase shift in the recycling cavity, given by

$$\frac{l_+ \omega_{\mathrm{m}}}{c} = \pi + 2k\pi\,, \tag{4}$$

for an integer k – hereafter we assume $k = 0$ for simplicity. Hence the nth-order sidebands acquire an additional round-trip phase shift of $n\pi$ in the recycling cavity. As a consequence, the odd-order sidebands resonate in the recycling cavity, while the even-order sidebands are anti-resonant, assuming that the asymmetry is small enough for the sidebands in question to contribute no sign change in reflection from the compound mirror.

The couplings of the carrier and the odd-order sidebands to the recycling cavity depends on the optical parameters. The amplitude reflectivity of the recycling cavity for the nth-order light ($r_{\mathrm{rec}\,n}$) is given by

$$r_{\mathrm{rec}\,n} = -r_{\mathrm{R}} + \frac{t_{\mathrm{R}}^2 r_{\mathrm{com}\,n}}{1 - r_{\mathrm{R}} r_{\mathrm{com}\,n}}\,, \tag{5}$$

where r_R and t_R are the reflectivity and the transmissivity of the recycling mirror. The reflectivity of the compound mirror ($r_{com\,n}$) is represented by

$$r_{com\,n} = (-1)^n t_P^2 r_{arm\,n} \cos n\alpha \,, \tag{6}$$

where t_P is the transmissivity of the pick-off mirror, and the parameter $\alpha \equiv l_- \omega_m/c$ represents the effect of the asymmetry for the sidebands. In order to maximize the carrier power gain in the recycling cavity, it is optimal for the carrier to be critically coupled to the recycling cavity; the reflectivity of the recycling mirror is set to be same as that of the compound mirror for the carrier, which is mainly determined by the loss in the arms and finite contrast. On the other hand, the coupling of the recycling cavity for the odd-order sidebands depends on the amount of the asymmetry. In practice, the optical parameters must be chosen by considering the robust extraction of the control signals, as described later. The factor g_n, given by

$$g_n = \frac{t_R}{1 - r_R r_{com\,n}} \,, \tag{7}$$

indicates the enhancement of the electric field on the beamsplitter by power recycling. As we mentioned, the second-order sidebands are not resonant with the recycling cavity; they are always under-coupled to the recycling cavity. The enhancement of the electric field for the second-order sidebands is much smaller than unity. We hence ignore g_2 in further calculations.

After experiencing a change of phase and amplitude in the interferometer, the sidebands produce intensity-modulated photocurrents at ω_m and its harmonics in the photodetectors. The information about the interferometer is acquired by demodulating these photocurrents. The conventional scheme uses demodulation at ω_m. When the initial phase of the local oscillator is the same as that of the modulation, we define it as *in-phase*, while the orthogonal demodulation phase is defined as *quadrature-phase*. The demodulated signals of the in-phase (I) and the quadrature-phase (Q) at the reflection port are given by the following linear combination of the deviation of each degree of freedom:

$$\begin{aligned} V_1^{(I)} = & -J_0(m) J_1(m)\, g_0^2 r_{rec\,1} |r'_{arm\,0}|\, \delta L_+ \\ & - J_0(m) J_1(m) \big(g_0^2 r_{rec\,1} r_{arm\,0} \\ & + g_1^2 r_{rec\,0} r_{arm\,1} \cos\alpha \big)\, \delta l_+ \end{aligned} \tag{8}$$

$$V_1^{(Q)} = -J_0(m) J_1(m)\, g_1^2 r_{rec\,0} r_{arm\,1} \sin\alpha\, \delta l_- \,. \tag{9}$$

Only the carrier and the first-order sidebands have been taken into account in this calculation for simplicity. Also, common factors such as the demodulation gain and the laser power have been omitted.

2.2. Problems of frontal modulation

Since only one phase modulation outside of the interferometer is needed to extract the signals necessary for the control, the frontal modulation scheme is considered as one of the most elegant techniques for extracting control signals of power-recycled Fabry–Perot–Michelson interferometers. However, there are several problems concerning the extraction of the δl_+ and δl_- signals.

One of the problems is that those demodulated signals which are sensitive to δl_+ have also high sensitivity to δL_+. The arm cavities enhance the phase shift of the carrier induced by the deviation of the arm lengths, resulting in large amplitudes of the signal corresponding to δL_+. This effect of the enhancement by the cavities at the reflection port is represented by $|r'_{arm\,0}|$ in the first term in Eq. (8). Typically, this first term is several hundreds times larger than the other terms for comparable fluctuations of δL_+ and δl_+. Because of this large contribution of δL_+, the stability of the control system is not ensured unless several restrictions are satisfied.

Another problem is that either the δl_+ signal or the δl_- signal can accidentally vanish under some conditions. The signal corresponding to δl_+ is extracted at the reflection port by means of the difference in the responses of the recycling cavity for the carrier and the first-order sidebands. Therefore, the term of the δl_+ signal in Eq. (8) vanishes when the responses of the recycling cavity become identical for the carrier and for the first-order sidebands. This condition is expressed as

$$r_{rec\,0} = r_{rec\,1} \,. \tag{10}$$

For the δl_- signal, the phase shift of the first-order sidebands by δl_- generates the signal when they interfere with the carrier at the reflection port. Therefore, the amplitude of the signal goes to zero when the carrier is critically coupled to the recycling cavity. This condition is given by

$$r_{\mathrm{rec}0} = 0 . \tag{11}$$

Although these conditions are, in practice, slightly affected by the signals produced by the higher-order sidebands which we ignored in Eqs. (8) and (9), the presence of these sidebands does not essentially change the situation described above.

When the interferometer is operated near these critical conditions, changes in the optical parameters can cause the feedback system to suffer from large variation of the signal sensitivities and even sign-reversals of the signals. Unfortunately, the optical parameters of the interferometer are usually designed not far from these conditions. When the loss for the carrier given by the arm cavities becomes comparative with the loss for the sidebands given by the asymmetry, the reflectivity of the recycling cavity for the first-order sidebands ($r_{\mathrm{rec}1}$) can be close to that for the carrier ($r_{\mathrm{rec}0}$). Also, the reflectivity of the recycling mirror is set so as to maximize the recycling gain for the carrier. The condition for this optimization is equivalent to Eq. (11). In order to avoid the instability of the control system, the actual optical parameters must be chosen carefully to have safety margins from these critical conditions against fluctuations of the optical parameters by, for instance, contamination of the mirror surfaces or misalignments of the mirrors.

3. New technique: signal extraction by $3\omega_{\mathrm{m}}$ demodulation

3.1. $3\omega_{\mathrm{m}}$ demodulation scheme

With our new technique, δl_+ and δl_- signals are extracted by demodulating the photocurrent at the reflection port using local oscillators at the third-harmonic frequency of the frontal phase modulation (Fig. 2, inside of the dashed box). This scheme improves the separation of δl_+ from δL_+, and ensures the robust extraction of δl_+ and δl_-. Moreover, this technique requires neither additional optical elements nor modification of the basic optical configuration as used in the conventional scheme.

The signals corresponding to δl_+ and δl_- with the $3\omega_{\mathrm{m}}$ demodulation are obtained at the in-phase and the quadrature-phase, respectively. The calculation of the signals naturally involves the second- and third-order sidebands which do not significantly contribute to the signal extraction with the conventional scheme. The $3\omega_{\mathrm{m}}$-demodulated signals are calculated as below:

$$\begin{aligned} V_3^{(\mathrm{I})} = & -J_0(m)\,J_3(m)\,g_0^2 r_{\mathrm{rec}3}|r'_{\mathrm{arm}0}|\,\delta L_+ \\ & - J_1(m)\,J_2(m)\,g_1^2 r_{\mathrm{rec}2} r_{\mathrm{arm}1}\cos\alpha\,\delta l_+ \\ & - J_0(m)\,J_3(m)\big(g_0^2 r_{\mathrm{rec}3} r_{\mathrm{arm}0} \\ & + g_3^2 r_{\mathrm{rec}0} r_{\mathrm{arm}3}\cos 3\alpha\big)\,\delta l_+ \end{aligned} \tag{12}$$

$$\begin{aligned} V_3^{(\mathrm{Q})} = & -J_1(m)\,J_2(m)\,g_1^2 r_{\mathrm{rec}2} r_{\mathrm{arm}1}\sin\alpha\,\delta l_- \\ & - J_0(m)\,J_3(m)\,g_3^2 r_{\mathrm{rec}0} r_{\mathrm{arm}3}\sin 3\alpha\,\delta l_- . \end{aligned} \tag{13}$$

The demodulated signals have several terms that arise from the beating of the carrier and the third-order sidebands and that of the first- and second-order sidebands. Since the carrier and the odd-order sidebands are resonant in the recycling cavity, both terms contribute to the δl_+ and δl_- signals. On the other hand, for the δL_+ signal, only the former term contributes to the signal because only the carrier carries the information of the arms.

In order to investigate the amplitudes of the signals with both of the ω_{m} and $3\omega_{\mathrm{m}}$ schemes, we introduce a realistic model of a large-scale interferometer, shown in Table 2. In the calculations, we have taken into account the higher-order sidebands up to second order for the signals with the ω_{m} scheme, while the sidebands up to third-order are taken into account for those with the $3\omega_{\mathrm{m}}$ scheme. Numerical calculations in the following sections are based on this model interferometer.

3.2. Reduction of the δL_+ signal at the reflection port

One of the advantages of the $3\omega_{\mathrm{m}}$ technique is that the δl_+ signal inherently has better separation from δL_+ compared with the ω_{m}-demodulated sig-

Table 2
The numerical parameters of the model interferometer used in the calculations.

	Symbol	Value
Modulation frequency	$\omega_m/2\pi$	15 MHz
Modulation index	m	0.8 rad
Arm length	L	3 km
Length of recycling cavity	$l_+/2$	5 m
Asymmetry	l_-	variable
Reflectivity of the front mirrors	r_F^2	0.97
Reflectivity of the end mirrors	r_E^2	0.9999
Reflectivity of the recycling mirror	r_R^2	variable
Transmissivity of the pick-off mirror	t_P^2	0.995
Loss of the mirrors		100 ppm
Reflectivity of AR coating		0.001

nal. In order to compare the separation of the δl_+ signal from δL_+ for each scheme, we introduce the separation ratio S_n for the $n\,\omega_m$ scheme, defined as

$$S_n = \frac{\partial_{\delta l_+} V_n^{(I)}}{\partial_{\delta L_+} V_n^{(I)}}\,, \tag{14}$$

where a bigger S_n means a better separation of the δl_+ signal. In Fig. 3, S_1 and S_3 for our model interferometer are plotted as functions of the asymmetry. In this calculation the reflectivity of the recycling mirror is 0.95 so that the recycling gain for the carrier is maximized. The separation is actually more than 30 times better with the $3\omega_m$ scheme when the asymmetry is smaller than 0.4 m. For some asymmetries either S_1 or S_3 becomes infinity. We will return to this point in Section 4.1.

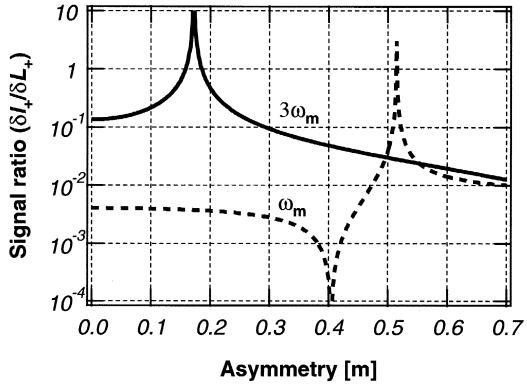

Fig. 3. The sensitivity ratio $\delta l_+/\delta L_+$ with the ω_m scheme (S_1, dashed line) and the $3\omega_m$ scheme (S_3, solid line) at the reflection port, as a function of the asymmetry. The sensitivity ratio is reduced with the $3\omega_m$ scheme when the asymmetry is smaller than 0.4 m. Each curve has a singular point where the signal ratio becomes particularly large (explained in Section 4.1).

By introducing very rough approximations, the separation of the δl_+ signals are considered for general sets of the optical parameters. Assuming a small asymmetry, i.e. $\alpha \ll 1$, the recycling factors are comparable for the carrier and the odd-order sidebands. The reflectivity of the recycling cavity for the non-resonant second-order sidebands is unity, while those for the other resonant sidebands are smaller than unity, i.e. $|r_{rec0}|, |r_{rec1}|, |r_{rec3}| \ll |r_{rec2}| \sim 1$. The reflectivities of the arm for both the carrier and the sidebands are assumed to be unity. According to these approximations, we can ignore the third term of Eq. (12) compared with the second term. After all, the comparison of the separations S_3/S_1 is simplified to the following expression:

$$\frac{S_3}{S_1} \sim \frac{J_1(m)\,J_2(m)}{J_0(m)\,J_3(m)}\,\frac{r_{rec1}}{r_{rec3}}\,\frac{g_1^2}{g_1^2 r_{rec0} - g_0^2 r_{rec1}}\,. \tag{15}$$

The leading factor $J_1(m)J_2(m)/J_0(m)J_3(m)$ is approximately equal to 3 when m is smaller than unity. The magnitude of the other part depends on the optical parameters. In general, when the asymmetry is small, S_3/S_1 tends to be large because of the S_3's dependence on g_1^2/r_{rec3}.

3.3. Amplitudes and signs of the signals with the $3\omega_m$ demodulation

Another advantage of the $3\omega_m$ demodulation is the robustness of the δl_+ and δl_- signals. The amplitudes and signs of the signals with the $3\omega_m$ demodulation are less dependent on the optical parameters than those with the conventional scheme. Furthermore the δl_+ and δl_- signals with the $3\omega_m$ scheme do not vanish for typical optical parameters. Thus, near the conditions represented by Eqs. (10) and (11), the amplitudes of the signals obtained with $3\omega_m$ scheme become larger than those with the conventional scheme.

Fig. 4 shows the amplitudes of the δl_+ signal with both schemes calculated for the model interferometer. In this calculation, the reflectivity of the recycling mirror has again been chosen to be 0.95. The ω_m signal vanishes for an asymmetry of 0.4 m. On the other hand, the $3\omega_m$ signal has only a mild dependence on the asymmetry, resulting in a larger δl_+ signal with the $3\omega_m$ scheme than with the ω_m scheme for asymmetries below 0.5 m.

Fig. 5 shows the amplitudes of the δl_- signal with both schemes. In this calculation, the reflectivity of the recycling mirror was varied around 0.95, where the carrier is critically coupled to the recycling cavity. With the ω_m demodulation, the amplitude of the δl_- signal highly depends on the reflectivity of the recycling mirror. For a reflectivity of 0.94, the signal completely vanishes. In this calculation the asymmetry is fixed at 0.3 m as an numerical example, though the situation is, in practice, hardly affected by choice of the asymmetry.

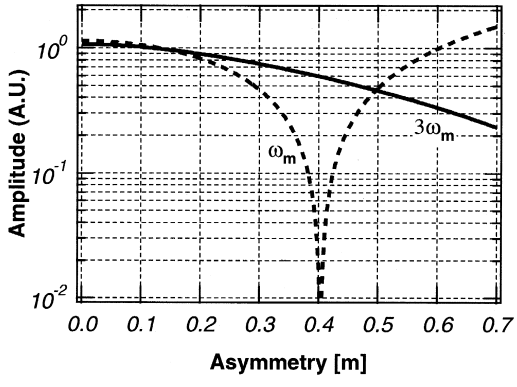

Fig. 4. Comparison of the amplitudes of the δl_+ signals with the ω_m scheme (dashed line) and the $3\omega_m$ scheme (solid line). Horizontal axis is the macroscopic asymmetry between the beamsplitter and the two front mirrors. In this calculation, the reflectivity of the recycling mirror has been chosen to be 0.95 so that the recycling gain for the carrier is maximized. The amplitude of the δl_+ signal with the ω_m scheme goes to zero at the asymmetry of 0.4 m, while that with the $3\omega_m$ scheme has a smaller dependence.

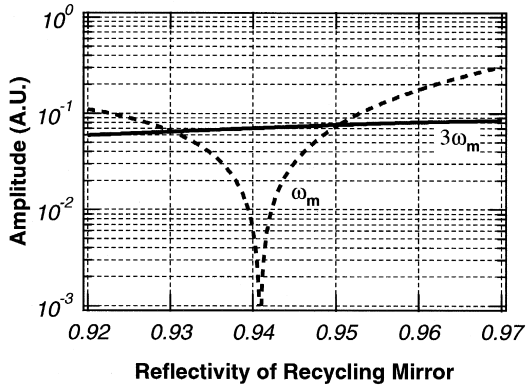

Fig. 5. Comparison of the amplitudes of the δl_- signals with the ω_m scheme (dashed line) and the $3\omega_m$ scheme (solid line). Horizontal axis is the reflectivity of the recycling mirror. In this calculation, the asymmetry is set to be 0.3 m. The amplitude of the δl_- signal with the ω_m scheme goes to zero at the reflectivity of 0.94, while that with the $3\omega_m$ scheme has a very weak dependence.

From the figures, one can see that the $3\omega_m$-demodulated signals do not vanish with typical optical parameters. This robustness of the signals is explained by two facts. First, these demodulated signals are not affected by the coupling of the carrier and the first-order sidebands to the recycling cavity because the presence of the carrier and the first-order sidebands are not essential in the signal extraction with the $3\omega_m$ scheme. Secondly, the amount of the second-order sidebands at the reflection port, which is essential for the $3\omega_m$ scheme, does not depend on the optical parameters because the second-order sidebands are not resonant in the recycling cavity.

We can compare the amplitudes of the signals with both schemes using the same approximations as used in the previous section. The ratios of the signal amplitudes with both schemes are defined as

$$S_+ = \frac{\partial_{\delta l_+} V_3^{(\mathrm{I})}}{\partial_{\delta l_+} V_1^{(\mathrm{I})}}, \quad S_- = \frac{\partial_{\delta l_-} V_3^{(\mathrm{Q})}}{\partial_{\delta l_-} V_1^{(\mathrm{Q})}}. \tag{16}$$

Using the approximations, S_+ and S_- can be expressed as

$$S_+ = \frac{J_2(m)}{J_0(m)} \frac{g_1^2}{g_1^2 r_{\mathrm{rec}0} - g_0^2 r_{\mathrm{rec}1}}, \tag{17}$$

$$S_- = \frac{J_2(m)}{J_0(m)} \frac{1}{r_{\mathrm{rec}0}}. \tag{18}$$

Both S_+ and S_- have the factor $J_2(m)/J_0(m)$ in common, which is about 0.09 for m of 0.8. Therefore, the amplitude of the signals with $3\omega_{\mathrm{m}}$ scheme are substantially smaller than those with the ω_{m} signals. Nevertheless, S_+ and S_- can be larger than unity because they also have an inverse-proportional dependency on $r_{\mathrm{rec}0}$ and $r_{\mathrm{rec}1}$; such situations are caused by the optical parameters near the conditions represented by Eqs. (10) and (11), as seen in the figures.

4. Discussions

4.1. Further reduction of δL_+

Since the enhancement of the δL_+ signal in the arm cavities is still large, the reflection port is not independent from δL_+ even with the $3\omega_{\mathrm{m}}$ scheme. We propose two techniques to further separate the δl_+ signal from δL_+. One is an optimization of the optical parameters to set the reflectivity of the recycling cavity for the third-order sidebands to be zero. The other is to remove the third-order sidebands from the injected light by applying a weak modulation at the $3\omega_{\mathrm{m}}$ frequency.

In the first technique, the δl_+ signal is separated by adjusting the optical parameters of the interferometer so that the interferometer does not reflect the third-order sidebands to the reflection port. This condition is represented by

$$r_{\mathrm{rec}3} = 0. \tag{19}$$

When this condition is realized, the contribution of δL_+ to the in-phase signal with the $3\omega_{\mathrm{m}}$ demodulation – which is proportional to $r_{\mathrm{rec}3}$ – is eliminated. This effect is seen in Fig. 3 as a singular point at the asymmetry of 0.17 m. This technique is an analogy to the signal separation technique for the ω_{m} demodulation that is reported in our earlier Letters [14,15]. In the original technique, the contribution of δL_+ is eliminated from the signal with the ω_{m} demodulation in the case of $r_{\mathrm{rec}1} = 0$, which corresponds to an asymmetry of 0.52 m. In general, Eq. (19) is satisfied with about one third of the asymmetry compared with the sideband elimination for the first-order sidebands. This may make it more difficult to obtain sufficient modulation sidebands at the detection port in the presence of contrast defect.

Since the contribution of δL_+ with the $3\omega_{\mathrm{m}}$ scheme is inherently smaller than that with the ω_{m} scheme, the required accuracy of the optical parameters for a certain separation ratio is relaxed compared with that for the ω_{m} scheme. In our model interferometer, the asymmetry must be set with an accuracy of 1.3 mm to obtain a sensitivity ratio of unity with the ω_{m} scheme. On the other hand, 27 mm is required with the $3\omega_{\mathrm{m}}$ scheme; the required accuracy in the optimization of the asymmetry is thus relaxed by a factor of 20.

Another approach for eliminating the δL_+ signal is to remove the third-order sidebands from the incident beam. This can be achieved by applying an additional weak phase modulation at $3\omega_{\mathrm{m}}$ with appropriate amplitude and phase. For instance, a modulation index of only 0.024 at $3\omega_{\mathrm{m}}$ cancels out $3\omega_{\mathrm{m}}$ sidebands caused by an ω_{m} modulation with a modulation index of 0.8. Although this technique requires an additional modulation to the input light, it has a great advantage that the δl_+ signal is separated from δL_+ without any tuning of the interferometer itself.

4.2. Experiment at the 3-m prototype interferometer

The technique using the $3\omega_{\mathrm{m}}$ demodulation is now being investigated with a 3-m prototype power-recycled Fabry–Perot–Michelson interferometer at the University of Tokyo [15–17]. This interferometer has its mirrors suspended in vacuum, and the optical configuration is very similar to the large-scale interferometers. We have already realized the stable operation of the 3-m prototype with the $3\omega_{\mathrm{m}}$ technique. The details of the experiment will be described in a future publication.

5. Conclusion

We have proposed a new signal extraction scheme for the control of power-recycled Fabry–Perot–Michelson interferometers with frontal modulation. In this technique the recycling cavity length (δl_+) and the Michelson path difference (δl_-) are extracted by demodulating the photocurrent at the reflection port with the third-harmonic frequency of the phase modulation. The technique can be realized by just putting additional demodulation circuits at the reflection port. The extracted signals are inherently less sensitive to the common motion of arm cavities (δL_+) than with the ordinary ω_m demodulation – the sensitivity to δL_+ is more than 30 times reduced for the model interferometer. As compared to the conventional scheme, the δl_+ and δl_- signals with the $3\omega_m$ scheme are less dependent on the optical parameters; the signals do not vanish for typical optical parameters, and the sign-reversals of the signals do not occur. As a result, the design of the optical parameters is greatly simplified with the $3\omega_m$ scheme.

We also propose two techniques for further separation of the δl_+ signal from δL_+ with the $3\omega_m$ scheme. One is to eliminate the third-order sidebands from the reflected light by optimizing the optical parameters. In our model, the required accuracy in the optimization of the asymmetry for the third-order sidebands is 20 times relaxed in comparison with the conventional scheme. Another technique is to remove the third-order sidebands from the input light by applying the weak modulation at $3\omega_m$. Although this technique requires the additional modulation, it has an advantage that the δl_+ signal is separated from δL_+ without any tuning of the interferometer itself.

The experimental study of the $3\omega_m$ scheme is now being carried out at the 3-m prototype interferometer at the University of Tokyo.

Acknowledgements

The authors would like to thank G. Heinzel and S. Kawamura for useful discussions. A part of this research is supported by a Grant-in-Aid for Creative Basic Research of the Ministry of Education (10NP0801).

References

[1] A. Abramovici, W.E. Althouse, R.W.P. Drever, Y. Gürsel, S. Kawamura, F.J. Raab, D. Shoemaker, L. Sievers, R.E. Spero, K.S. Thorne, R.E. Vogt, R. Weiss, S.E. Whitcomb, M.E. Zucker, Science 256 (1992) 325.
[2] VIRGO Collaboration, VIRGO Final Conceptual Design, 1992.
[3] K. Danzmann, H. Lück, A. Rüdiger, R. Schilling, M. Schrempel, W. Winkler, J. Hough, G.P. Newton, N.A. Robertson, H. Ward, A.M. Campbell, J.E. Logan, D.I. Robertson, K.A. Strain, J.R.J. Bennett, V. Kose, M. Kühne, B.F. Schutz, D. Nicholson, J. Shuttleworth, H. Welling, P. Aufmuth, R. Rinkleff, A. Tünnermann, B. Willke, Proposal for a 600m Laser-Interferometric Gravitational Wave Antenna, Max-Planck-Institut für Quantenoptik Report 190, Garching, Germany, 1994.
[4] K. Tsubono, 300-m laser interferometer gravitational wave detector (TAMA300) in Japan, in: E. Coccia, G. Pizzella, F. Ronga (Eds.), Proc. First E. Amaldi Conf. on Gravitational Wave Experiments, June 1994, World Scientific, Singapore, 1995, p. 112.
[5] R.W.P. Drever, Fabry–Perot cavity gravity-wave detectors, The detection of gravitational waves, D.G. Blair (Ed.), Cambridge Univ. Press, Cambridge, 1991, p. 306.
[6] M.W. Regehr, Signal extraction and control for an interferometric gravitational wave detector, Ph.D. thesis, California Institute of Technology, 1995.
[7] M.W. Regehr, F.J. Raab, S.E. Whitcomb, Opt. Lett. 20 (1995) 1507.
[8] R. Flaminio, H. Heitmann, Phys. Lett. A 214 (1996) 112.
[9] R.W.P. Drever, J.L. Hall, F.V. Kowalski, J. Hough, G.M. Ford, A.J. Munley, H. Ward, Appl. Phys. B 31 (1983) 97.
[10] L. Schnupp, talk at European Collaboration Meeting on Interferometric detection of gravitational waves, Sorrent, 1988.
[11] R. Takahashi, J. Mizuno, S. Miyoki, N. Kawashima, Phys. Lett. A 187 (1994) 157.
[12] J.A. Giaime, Studies of laser interferometer design and a vibration isolation system for interferometric gravitational wave detectors, Ph.D. thesis, Massachusetts Institute of Technology, 1995.
[13] D. Sigg, N. Mavalvala, J.A. Giaime, P. Fritschel, D. Shoemaker, Appl. Opt. 37 (1998) 5687.
[14] M. Ando, K. Kawabe, K. Tsubono, Phys. Lett. A 237 (1997) 13.
[15] M. Ando, K. Arai, K. Kawabe, K. Tsubono, Phys. Lett. A 268 (2000) 268.
[16] K. Kawabe, S. Nagataki, M. Ando, K. Tochikubo, N. Mio, K. Tsubono, Appl. Phys. B 62 (1996) 135.
[17] M. Ando, K. Arai, K. Kawabe, K. Tsubono, Phys. Lett. A 248 (1998) 145.